Electron Dominated Thermoelectric Response in MNiSn (M:Ti,Zr,Hf) Half-Heusler Alloys

Journal:	*Physical Chemistry Chemical Physics*
Manuscript ID	CP-ART-03-2016-001786.R1
Article Type:	Paper
Date Submitted by the Author:	08-Apr-2016
Complete List of Authors:	Gandi, Appala Naidu; KAUST, Materials Science and Engineering Schwingenschlogl, Udo; KAUST,

Electron Dominated Thermoelectric Response in MNiSn (M:Ti,Zr,Hf) Half-Heusler Alloys

Appala Naidu Gandi and Udo Schwingenschlögl*

King Abdullah University of Science and Technology (KAUST), Physical Sciences and Engineering Division (PSE), Thuwal 23955-6900, Saudi Arabia

E-mail: udo.schwingenschlogl@kaust.edu.sa

Abstract

We solve the transport equations of the electrons and phonons to understand the thermoelectric behaviour of the technologically important half-Heusler alloys MNiSn (M:Ti,Zr,Hf). Doping is simulated within the rigid band approximation. We clarify the origin of the electron dominated thermoelectric response and determine the carrier concentrations with maximal figures of merit. The phonon mean free path is studied to calculate the grain size below that grain refinement methods can enforce ballistic heat conduction to enhance the figure of merit.

Keywords

half-Heusler alloy, thermal conductivity, thermoelectrics, Seebeck coefficient, phonon mean free path

Introduction

MNiSn alloys are explored for thermoelectric applications because of their environmental friendliness, high temperature stability, and straight forward synthesis.[1] They have narrow bandgaps and cubic $F\bar{4}3m$ structures (MgAgAs-type)[2] with the M, Ni, and Sn atoms occupying the 4*b*, 4*c*, and 4*a* Wyckoff positions, respectively, leaving the 4*d* site vacant. Since the figure of merit ($zT = S^2\sigma T/\kappa$) is related to the Seebeck coefficient (S), electrical conductivity (σ), and thermal conductivity (κ), fundamental understanding of the electron and phonon transport processes is necessary for improving the thermoelectric performance.

Photoemission spectra[3] and structural refinement studies[4,5] suggest that Ni occupies $\approx 2\%$ of the 4*d* sites and results in in-gap states responsible for the excellent thermoelectric behaviour. Despite various efforts there still seems to be disagreement in the literature about the exact value of the bandgap.[6–9] For n-doped samples values of up to $zT = 0.81$ have been reported,[10] whereas p-doped samples, which can be achieved by partial replacement of Ni with Co/Ir[11,12] or of Ti/Zr with Sc/Y,[13,14] show $zT < 0.31$.[15] Most of the alloys show at high temperature electron dominated thermoelectric response.[11–13] As a consequence, the thermoelectric potential of p-doped samples (50% larger peak powerfactors than for n-doping predicted by first-principles calculations[16]) cannot be used.

The high thermal conductivities in the large grain limit (TiNiSn: 9.3 $\mathrm{Wm^{-1}K^{-1}}$,[13] ZrNiSn: 17.2 $\mathrm{Wm^{-1}K^{-1}}$,[17] HfNiSn: 12.8 $\mathrm{Wm^{-1}K^{-1}}$ [17]) can be overcome by grain refinement (to increase the boundary scattering)[18–20] and alloying (to increase the mass fluctuation scattering)[10,13,17,21–24] methods. A systematic improvement of the thermal conductivity is not possible, because the roles of the different phonon modes are not known, even though the lattice contribution to the thermal conductivity has been estimated for TiNiSn[25,26] and ZrNiSn.[26] The aim of the present study therefore is not only to clarify the origin of the electron dominated thermoelectric response but also to provide detailed insight into the lattice thermal conductivity.

Methodology

First-principles calculations are performed using the Vienna Ab-initio Simulation Package.[27] Plane waves with energies up to 300 eV are employed in the expansion of the electronic wave functions, considering the Ti $3d, 4s$, Zr $4s, 4p, 4d, 5s$, Hf $5d, 6s$, Ni $3d$, $4s$, and Sn $5s$, $5p$ states as valence states. We employ the generalised gradient approximation of the exchange-correlation potential in the Perdew-Burke-Ernzerhof flavour. Brillouin zone integrations are performed using the tetrahedron method with Blöchl corrections.[28] Γ-centered $24 \times 24 \times 24$ k-meshes are used for optimising the structures. For all systems under consideration spin-degenerate states are obtained.

We solve the semi-classical Boltzmann transport equation within the constant relaxation time approximation for calculating S, σ, and the electronic contribution to κ. A rigid band approximation is used to simulate doping (BoltzTraP code[29]), i.e., it is assumed that the doping does not modifiy the host band structure but only shifts the chemical potential. For this purpose, the electronic band structure is calculated on a very fine $44 \times 44 \times 44$ k-mesh. Even five times denser meshes are used in the Fourier expansion of the electronic band energies. We use a constant relaxation time of $\tau = 1.5 \times 10^{-14}$ s, as obtained by comparing σ/τ to the experiment (sample 5 in Ref. 30).

The normal mode polarisation vectors and phonon frequencies are calculated within the harmonic approximation.[31] A $2 \times 2 \times 2$ supercell of the conventional unit cell is employed with a $3 \times 3 \times 3$ k-mesh for evaluating the forces. Long range dipole interactions are included in the dynamical matrix.[32] The dielectric tensor and Born effective charges are evaluated using perturbation theory.[33] In addition, we employ a finite difference scheme for calculating the third order force constants,[34] where each atom up to fourth nearest neighbours is simultaneously displaced with a given atom (interaction distance up to 6.4 Å). Translational invariance is imposed on the force constants.[35] Second and third order force constants are used for solving a linearised Boltzmann transport equation self-consistently by the Sheng-BTE code.[36,37] For this purpose, Brillouin zone integrations are carried out on $14 \times 14 \times 14$

Table 1: Lattice constant (experimental values from Ref. 2), bandgap, high frequency dielectric tensor (xx component), and in-plane Born effective charges (in electrons).

	TiNiSn	ZrNiSn	HfNiSn
a, theoretical (Å)	5.942	6.147	6.107
a, experimental (Å)	5.941	6.113	6.083
bandgap (eV)	0.44	0.49	0.36
ε^{∞}	24.56	21.98	20.82
Z^*_{M}	2.87	2.61	2.74
Z^*_{Ni}	−4.01	−3.63	−3.66
Z^*_{Sn}	1.14	1.02	0.92

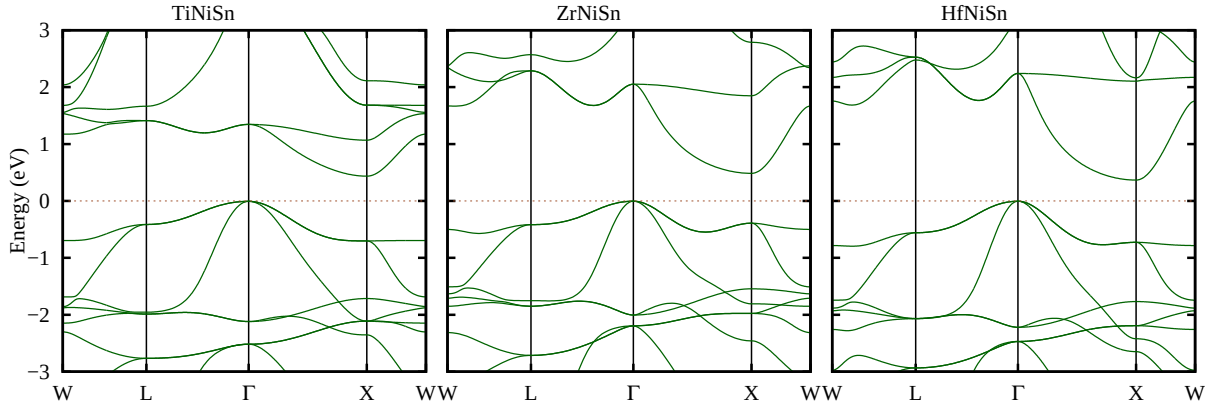

Figure 1: Electronic band structures.

k-meshes. For temperatures above the Debye temperature (TiNiSn: 283 K, ZrNiSn: 310 K, HfNiSn: 255 K[8]) and clearly below the melting point (TiNiSn: 1453 K, ZrNiSn: 1708 K, HfNiSn: 1760 K[38]), κ is determined by three phonon Umklapp scattering events[39] and our methodology therefore gives valid results. The three compounds under study show their optimal thermoelectric performance around 700 K (because at higher temperatures κ increases due to ambipolar diffusion[10,23,40–42]).

Results and discussion

The optimized lattice constants are compared with experimental values in Table 1, showing good agreement. The electronic band structures in Figure 1 reveal in each case an indirect

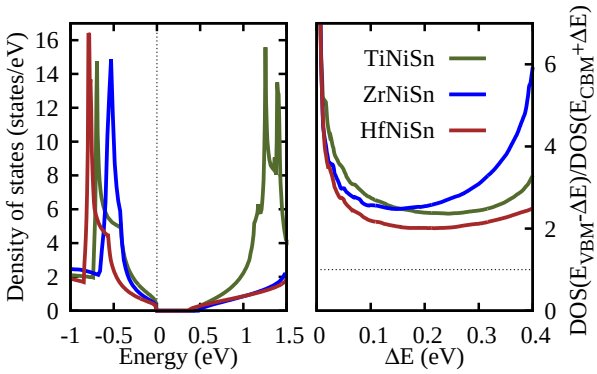

Figure 2: Densities of states (left) and ratios at the band edges (right).

Table 2: Effective mass in units of the free electron mass.

Band	Direction	TiNiSn	ZrNiSn	HfNiSN
VBM1	$\Gamma \leftrightarrow$ L	0.39	0.25	0.22
VBM1	$\Gamma \leftrightarrow$ X	0.64	0.40	0.38
VBM2, VBM3	$\Gamma \leftrightarrow$ L	3.72	2.44	2.11
VBM2, VBM3	$\Gamma \leftrightarrow$ X	1.30	0.88	0.71
CBM	X $\leftrightarrow \Gamma$	2.89	3.23	3.14
CBM	X $\leftrightarrow$ W	0.56	0.38	0.36

bandgap with a triple degenerate valence band maximum (VBM) at the Γ point and the conduction band minimum (CBM) at the X point. Correspondingly, the density of states (DOS) at the valence band edge is larger than that at the conduction band edge, see Figure 2. Analysis of the partial DOS (not shown) demonstrates that the VBM is formed by the M d states and the CBM by the M d and Ni 3d states. The distinct DOS peak around -0.5 eV is due to hybridized M d, Ni 3d, and Sn 5p states. All these results agree well with the existing literature.[43] We number the bands forming the VBM in order of increasing energy around the Γ point (VBM1, VBM2, and VBM3) and summarize in Table 2 the obtained carrier effective masses. The heavy holes in the flat band VBM1 enhance S, whereas the light holes in the bands VBM2 and VBM3 dominate σ. This combination leads to high powerfactors in the case of p-doping, see Figure 3.

Figure 4(bottom) shows the variation of the Fermi level μ with the temperature. For low temperature it is located close to the CBM/VBM for n/p doping. Since the occupation

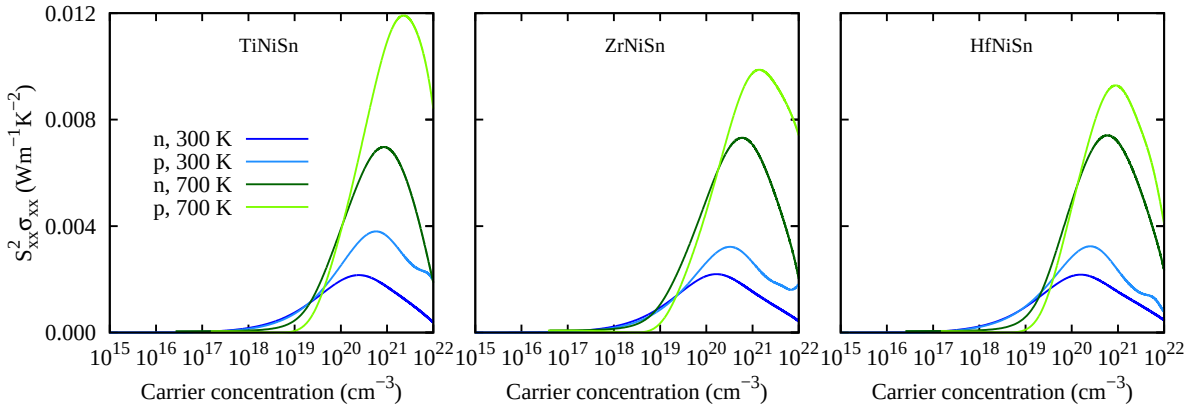

Figure 3: Power factors as functions of the carrier concentration.

of states above/below the CBM/VBM increases/decreases with increasing temperature, μ shifts toward the middle of the bandgap (extrinsic region). For low carrier concentration the minority carriers start playing a role around 170 K, see Figure 4(top), and μ therefore shows a crossover into a linear regime (intrinsic/bipolar region). In this regime the thermoelectric response turns out to be electron dominated (μ located above the middle of the bandgap), because the DOS at $E_{\mathrm{VBM}} - \Delta E$ (valence states) is much higher than at $E_{\mathrm{CBM}} + \Delta E$ (conduction states), see Figure 2(right). For the same reason, μ is characterized by a remarkably high slope as function of the temperature, see Figure 4(bottom). The higher the carrier concentration the deeper μ initially is located in the conduction/valence band (n/p-doping). For increasing temperature it approaches the value obtained for low carrier concentration, as expected. Figure 4 agrees in this sense for n-doping with the observed decrease of μ between 20 K to 100 K in ZrNiSn[44] and with Figure 3 in Ref. 45.

When both electrons (e) and holes (h) participate in the thermoelectric response, we have $S = (S_e\sigma_e + S_h\sigma_h)/(\sigma_e + \sigma_h)$ with $S_e < 0$ and $S_h > 0$.[46] At low temperature the thermoelectric response is due to only one type of carrier (extrinsic region). Therefore, |S| first increases with the temperature but then reaches a maximum ($|\mathrm{S}|_{max}$, T_{max}) as the other type of carriers starts to contribute significantly (bipolar/intrinsic region). These features are clearly seen in Figure 4. For n-doping S remains negative above T_{max}, since μ remains above the middle of the bandgap. The thermoelectric response therefore is electron dominated. While strongly

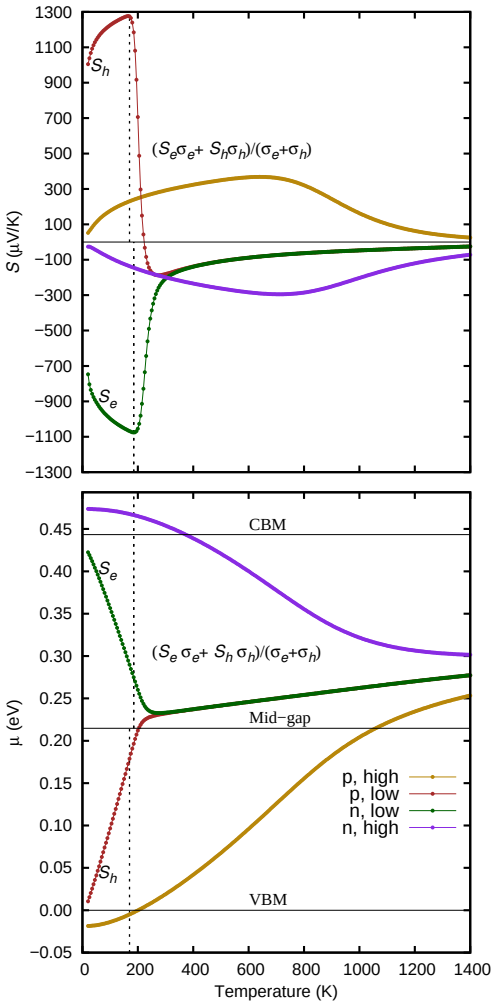

Figure 4: Seebeck coefficient and Fermi level as functions of the temperature for low (10^{15} cm^{-3}) and high (10^{20} cm^{-3}) doped (n and p) TiNiSn.

p-doped samples behave analogous to strongly n-doped samples, a different behaviour is found for weak p-doping, see Figure 4. At a certain temperature, S becomes negative even though the hole concentration exceeds the electron concentration, which is again a consequence of the fact that μ is located above the middle of the bandgap. Such transitions have been observed experimentally in $ZrNi_{1-y}Co_ySn$ for $y = 0.04$ to 0.12,[12] $Zr_{0.98}Y_{0.02}NiSn$,[13] $Hf_{0.75}Zr_{0.25}Ni_{0.95}Co_{0.05}Sn$,[11] $Zr_{1-x}Sc_xNiSn$ for $x = 0.02$ to 0.04,[9] and $TiNiCo_ySn$ for $y = 0.025$ to 0.075.[5] Figure 4 demonstrates that the sign of S in the present class of alloys only reflects the nature of the *dominating* carriers and not that of the *majority* carriers.

The Goldsmid-Sharp formula[46] gives for the bandgap the values $(2e|S|_{max}T_{max})$ summa-

Table 3: Peak Seebeck coefficients, corresponding temperatures, and bandgaps estimated with the Goldsmid-Sharp formula.

	Doping (cm^{-3})	$\|S\|_{max}$ (μV/K)	T_{max} (K)	$2e\|S\|_{max}T_{max}$ (eV)
TiNiSn	n: 10^{15}, 10^{17}, 10^{19}	1088, 760, 435	185, 260, 460	0.40, 0.40, 0.40
	p: 10^{15}, 10^{17}, 10^{19}	1248, 858, 519	170, 245, 425	0.42, 0.42, 0.44
ZrNiSn	n: 10^{15}, 10^{17}, 10^{19}	1094, 745, 422	205, 300, 535	0.45, 0.45, 0.45
	p: 10^{15}, 10^{17}, 10^{19}	1182, 825, 490	195, 280, 490	0.46, 0.46, 0.48
HfNiSn	n: 10^{15}, 10^{17}, 10^{19}	1028, 707, 389	165, 235, 440	0.34, 0.33, 0.34
	p: 10^{15}, 10^{17}, 10^{19}	1183, 784, 450	150, 225, 410	0.36, 0.35, 0.37

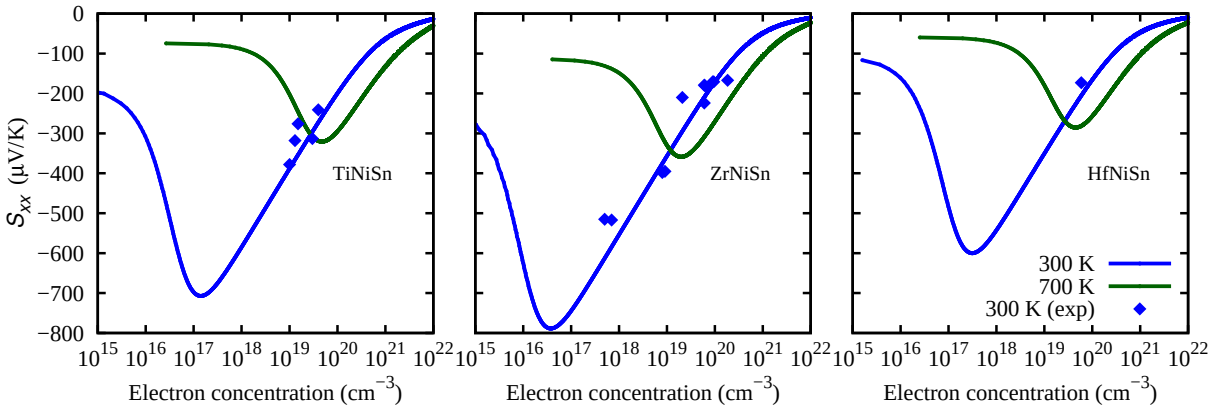

Figure 5: Seebeck coefficients as functions of the electron concentration. The experimental data are taken from Refs. 15,17,24,30,44,47,48.

rized in Table 3. They lie within ±10% of the calculated bandgap despite the non-parabolic nature of the electronic bands. Figure 5 shows S as a function of the temperature for different carrier concentrations and demonstrates excellent agreement with experimental results for n-doped samples.[15,17,24,30,44,47,48]

The high frequency dielectric tensors and Born effective charges reported in Table 1 are used along with the second order force constants to determine the harmonic phonon dispersion relations. The resulting lattice contributions to the thermal conductivity are plotted in Figure 6. Fitting by the relation $\kappa^{latt} \propto 1/T$ gives almost perfect agreement, which demonstrates that κ is limited by Umklapp scattering.[49] Figure 6 also shows that most of the heat conduction happens through acoustic phonons. At room temperature we obtain for κ^{latt} values of 13.4 $Wm^{-1}K^{-1}$ for TiNiSn, 14.4 $Wm^{-1}K^{-1}$ for ZrNiSn, and 14.4

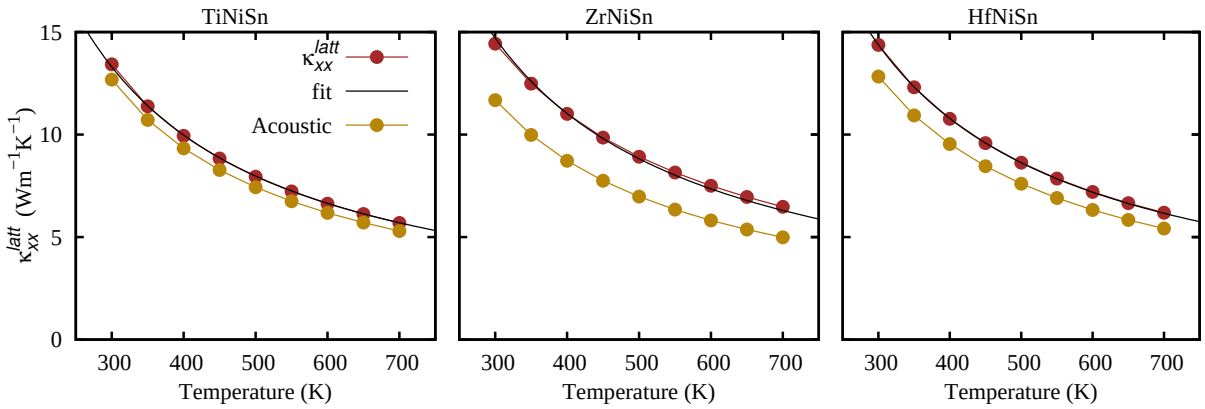

Figure 6: Lattice contributions to the thermal conductivity as functions of the temperature.

Table 4: Maximal figure of merit, corresponding carrier concentration, and maximal phonon mean free path at 300 K and 700 K.

		p-doping ($\times 10^{20}$ cm^{-3})	zT	n-doping ($\times 10^{20}$ cm^{-3})	zT	Λ_{max} (nm)
300 K	TiNiSn	4.6	0.07	2.1	0.04	1233
	ZrNiSn	3.2	0.06	1.5	0.04	1238
	HfNiSn	2.4	0.06	1.5	0.04	1485
700 K	TiNiSn	7.1	0.46	3.6	0.36	403
	ZrNiSn	4.8	0.41	2.2	0.35	486
	HfNiSn	3.6	0.40	2.2	0.35	586

Wm^{-1}K^{-1} for HfNiSn. For ZrNiSn this result fits well to the experimental single crystal value of $\kappa = 18$ Wm^{-1}K^{-1} [30]), since κ^{latt} is expected to dominate in semiconductors.

The possible effects of grain refinement are studied by expressing the contributions to κ in terms of polarisation averaged phonon mean free paths. When the grain size is less than the largest phonon mean free path, Λ_{max}, boundary scattering becomes dominant. The effective phonon mean free paths span a range of three orders of magnitude, see Table 4. Grain refinement below Λ_{max} will reduce κ^{latt}. The maximal achievable values of zT and the required carrier concentrations are listed in Table 4. These values correspond to large grains with only diffusive heat transfer. Since the mean free paths of the electrons are smaller than those of the phonons,[50] improvement of zT can be achieved by grain refinement below Λ_{max}, because the boundary scattering reduces κ^{latt} without affecting σ. Due to the larger

powerfactors, see Figure 3, p-doping gives a slightly better thermoelectric performance than n-doping, but high p-doping levels could not be achieved experimentally so far.

Conclusions

We have solved the Boltzmann transport equations for the electrons and phonons to study the electron dominated thermoelectric response in the MNiSn (M:Ti,Zr,Hf) alloys. Previous experimental observations are explained in terms of the doping and temperature dependences of the position of the Fermi level with respect to the band edges. Since the Fermi level shifts at elevated temperatures with an unusally high slope towards the conduction band minimum, the electron dominated thermoelectric response can be overcome only by a high hole concentration to realise an efficient p-type thermoelectric material. Analysis of the phonon mean free paths provides guide to grain refinement methods, as the grain sizes below which the heat conduction becomes ballistic (and the thermoelectric performance therefore can be enhanced by such methods) are determined.

Acknowledgements

The research reported in this publication was supported by funding from King Abdullah University of Science and Technology (KAUST). Computational resources were provided by the Supercomputing Laboratory of KAUST.

References

(1) Birkel, C. S.; Zeier, W. G.; Douglas, J. E.; Lettiere, B. R.; Mills, C. E.; Seward, G.; Birkel, A.; Snedaker, M. L.; Zhang, Y.; Snyder, G. J.; Pollock, T. M.; Seshadri, R.; Stucky, G. D. Rapid Microwave Preparation of Thermoelectric TiNiSn and TiCoSb Half-Heusler Compounds. *Chem. Mater.* **2012**, *24*, 2558–2565.

(2) Jeitschko, W. Transition Metal Stannides with MgAgAs and $MnCu_2Al$ Type Structure. *Metall. Trans.* **1970**, *1*, 3159–3162.

(3) Miyamoto, K.; Kimura, A.; Sakamoto, K.; Ye, M.; Cui, Y.; Shimada, K.; Namatame, H.; Taniguchi, M.; Fujimori, S.-I.; Saitoh, Y.; Ikenaga, E.; Kobayashi, K.; Tadano, J.; Kanomata, T. In-Gap Electronic States Responsible for the Excellent Thermoelectric Properties of Ni-Based Half-Heusler Alloys. *Appl. Phys. Express* **2008**, *1*, 081901.

(4) Downie, R. A.; MacLaren, D. A.; Smith, R. I.; Bos, J. W. G. Enhanced Thermoelectric Performance in TiNiSn-Based Half-Heuslers. *Chem. Commun.* **2013**, *49*, 4184–4186.

(5) Downie, R. A.; Smith, R. I.; MacLaren, D. A.; Bos, J.-W. G. Metal Distributions, Efficient n-Type Doping, and Evidence for In-Gap States in $TiNiM_ySn$ (M = Co, Ni, Cu) Half-Heusler Nanocomposites. *Chem. Mater.* **2015**, *27*, 2449–2459.

(6) Aliev, F. G.; Brandt, N. B.; Moshchalkov, V. V.; Kozyrkov, V. V.; Skolozdra, R. V.; Belogorokhov, A. I. Gap at the Fermi Level in the Intermetallic Vacancy System RBiSn (R=Ti,Zr,Hf). *Z. Phys. B Con. Mat.* **1989**, *75*, 167–171.

(7) Aliev, F. G.; Kozyrkov, V. V.; Moshchalkov, V. V.; Scolozdra, R. V.; Durczewski, K. Narrow Band in the Intermetallic Compounds MNiSn (M=Ti, Zr, Hf). *Z. Phys. B Con. Mat.* **1990**, *80*, 353–357.

(8) Aliev, F. G. Gap at Fermi Level in Some New d- and f-Electron Intermetallic Compounds. *Physica B: Condens. Matter* **1991**, *171*, 199–205.

(9) Schmitt, J.; Gibbs, Z. M.; Snyder, G. J.; Felser, C. Resolving the True Band Gap of ZrNiSn Half-Heusler Thermoelectric Materials. *Mater. Horiz.* **2014**, *2*, 68–75.

(10) Culp, S. R.; Poon, S. J.; Hickman, N.; Tritt, T. M.; Blumm, J. Effect of Substitutions on the Thermoelectric Figure of Merit of Half-Heusler Phases at 800 °C. *Appl. Phys. Lett.* **2006**, *88*, 042106.

(11) Simonson, J. W.; Poon, S. J. Electronic Structure of Transition Metal-Doped XNiSn and XCoSb (X = Hf,Zr) Phases in the Vicinity of the Band Gap. *J. Phys.: Condens. Matter* **2008**, *20*, 255220.

(12) Xie, H.-H.; Yu, C.; He, B.; Zhu, T.-J.; Zhao, X.-B. Thermoelectric Properties and n- to p-Type Conversion of Co-Doped ZrNiSn-Based Half-Heusler Alloys. *J. Electron. Mater.* **2012**, *41*, 1826–1830.

(13) Hohl, H.; Ramirez, A. P.; Goldmann, C.; Ernst, G.; Wölfing, B.; Bucher, E. Efficient Dopants for ZrNiSn-Based Thermoelectric Materials. *J. Phys.: Condens. Matter* **1999**, *11*, 1697.

(14) Horyn', A.; Bodak, O.; Romaka, L.; Gorelenko, Y.; Tkachuk, A.; Davydov, V.; Stadnyk, Y. Crystal Structure and Physical Properties of (Ti,Sc)NiSn and (Zr,Sc)NiSn Solid Solutions. *J. Alloys Compd.* **2004**, *363*, 10–14.

(15) Kimura, Y.; Tanoguchi, T.; Kita, T. Vacancy Site Occupation by Co and Ir in Half-Heusler ZrNiSn and Conversion of the Thermoelectric Properties from n-Type to p-Type. *Acta Mater.* **2010**, *58*, 4354–4361.

(16) Yang, J.; Li, H.; Wu, T.; Zhang, W.; Chen, L.; Yang, J. Evaluation of Half-Heusler Compounds as Thermoelectric Materials Based on the Calculated Electrical Transport Properties. *Adv. Funct. Mater.* **2008**, *18*, 2880–2888.

(17) Uher, C.; Yang, J.; Hu, S.; Morelli, D. T.; Meisner, G. P. Transport Properties of Pure and Doped MNiSn (M=Zr, Hf). *Phys. Rev. B* **1999**, *59*, 8615–8621.

(18) Bhattacharya, S.; Tritt, T. M.; Xia, Y.; Ponnambalam, V.; Poon, S. J.; Thadhani, N. Grain Structure Effects on the Lattice Thermal Conductivity of Ti-Based Half-Heusler Alloys. *Appl. Phys. Lett.* **2002**, *81*, 43–45.

(19) Zou, M.; Li, J.-F.; Du, B.; Liu, D.; Kita, T. Fabrication and Thermoelectric Properties of Fine-Grained TiNiSn Compounds. *J. Solid State Chem.* **2009**, *182*, 3138–3142.

(20) Yu, C.; Zhu, T.-J.; Xiao, K.; Shen, J.-J.; Yang, S.-H.; Zhao, X.-B. Reduced Grain Size and Improved Thermoelectric Properties of Melt Spun (Hf,Zr)NiSn Half-Heusler Alloys. *J. Electron. Mater.* **2009**, *39*, 2008–2012.

(21) Bhattacharya, S.; Pope, A. L.; Iv, R. T. L.; Tritt, T. M.; Ponnambalam, V.; Xia, Y.; Poon, S. J. Effect of Sb Doping on the Thermoelectric Properties of Ti-Based Half-Heusler Compounds, $TiNiSn_{1-x}Sb_x$. *Appl. Phys. Lett.* **2000**, *77*, 2476–2478.

(22) Shen, Q.; Chen, L.; Goto, T.; Hirai, T.; Yang, J.; Meisner, G. P.; Uher, C. Effects of Partial Substitution of Ni by Pd on the Thermoelectric Properties of ZrNiSn-Based Half-Heusler Compounds. *Appl. Phys. Lett.* **2001**, *79*, 4165–4167.

(23) Sakurada, S.; Shutoh, N. Effect of Ti Substitution on the Thermoelectric Properties of (Zr,Hf)NiSn Half-Heusler Compounds. *Appl. Phys. Lett.* **2005**, *86*, 082105.

(24) Kim, S.-W.; Kimura, Y.; Mishima, Y. High Temperature Thermoelectric Properties of TiNiSn-Based Half-Heusler Compounds. *Intermetallics* **2007**, *15*, 349–356.

(25) Ding, G.; Gao, G. Y.; Yao, K. L. Examining the Thermal Conductivity of the Half-Heusler Alloy TiNiSn by First-Principles Calculations. *J. Phys. D: Appl. Phys.* **2015**, *48*, 235302.

(26) Carrete, J.; Li, W.; Mingo, N.; Wang, S.; Curtarolo, S. Finding Unprecedentedly Low-Thermal-Conductivity Half-Heusler Semiconductors via High-Throughput Materials Modeling. *Phys. Rev. X* **2014**, *4*, 011019.

(27) Kresse, G.; Furthmüller, J. Efficient Iterative Schemes for Ab Initio Total-Energy Calculations Using a Plane-Wave Basis Set. *Phys. Rev. B* **1996**, *54*, 11169–11186.

(28) Blöchl, P. E.; Jepsen, O.; Andersen, O. K. Improved Tetrahedron Method for Brillouin-Zone Integrations. *Phys. Rev. B* **1994**, *49*, 16223–16233.

(29) Madsen, G. K. H.; Singh, D. J. BoltzTraP. A Code for Calculating Band-Structure Dependent Quantities. *Comput. Phys. Commun.* **2006**, *175*, 67–71.

(30) Kafer, W.; Fess, K.; Kloc, C.; Friemelt, K.; Bucher, E. Thermoelectric Properties of MNiSn (M=Ti,Zr,Hf) Single Crystals and Related Alloys. XVI International Conference on Thermoelectrics, 1997. Proceedings ICT '97. 1997; pp 489–492.

(31) Alfè, D. PHON: A Program to Calculate Phonons Using the Small Displacement Method. *Comput. Phys. Commun.* **2009**, *180*, 2622–2633.

(32) Cochran, W.; Cowley, R. A. Dielectric Constants and Lattice Vibrations. *J. Phys. Chem. Solids* **1962**, *23*, 447–450.

(33) Baroni, S.; Giannozzi, P.; Testa, A. Green's-Function Approach to Linear Response in Solids. *Phys. Rev. Lett.* **1987**, *58*, 1861–1864.

(34) Esfarjani, K.; Stokes, H. T. Method to Extract Anharmonic Force Constants from First Principles Calculations. *Phys. Rev. B* **2008**, *77*, 144112.

(35) Li, W.; Lindsay, L.; Broido, D. A.; Stewart, D. A.; Mingo, N. Thermal Conductivity of Bulk and Nanowire $Mg_2Si_xSn_{1-x}$ Alloys from First Principles. *Phys. Rev. B* **2012**, *86*, 174307.

(36) Li, W.; Mingo, N.; Lindsay, L.; Broido, D. A.; Stewart, D. A.; Katcho, N. A. Thermal Conductivity of Diamond Nanowires from First Principles. *Phys. Rev. B* **2012**, *85*, 195436.

(37) Li, W.; Carrete, J.; A. Katcho, N.; Mingo, N. ShengBTE: A Solver of the Boltzmann Transport Equation for Phonons. *Comput. Phys. Commun.* **2014**, 1747–1758.

(38) Jung, D.; Kurosaki, K.; Kim, C.; Muta, H.; Yamanaka, S. Thermal Expansion and Melting Temperature of the Half-Heusler Compounds: MNiSn (M = Ti, Zr, Hf). *J. Alloys Compd.* **2010**, *489*, 328–331.

(39) Ecsedy, D. J.; Klemens, P. G. Thermal Resistivity of Dielectric Crystals Due to Four-Phonon Processes and Optical Modes. *Phys. Rev. B* **1977**, *15*, 5957–5962.

(40) Muta, H.; Kanemitsu, T.; Kurosaki, K.; Yamanaka, S. Substitution Effect on Thermoelectric Properties of ZrNiSn Based Half-Heusler Compounds. *Mater. Trans.* **2006**, *47*, 1453–1457.

(41) Yu, C.; Zhu, T.-J.; Shi, R.-Z.; Zhang, Y.; Zhao, X.-B.; He, J. High-Performance Half-Heusler Thermoelectric Materials $Hf_{1-x}Zr_xNiSn_{1-y}Sb_y$ Prepared by Levitation Melting and Spark Plasma Sintering. *Acta Mater.* **2009**, *57*, 2757–2764.

(42) Douglas, J. E.; Birkel, C. S.; Verma, N.; Miller, V. M.; Miao, M.-S.; Stucky, G. D.; Pollock, T. M.; Seshadri, R. Phase Stability and Property Evolution of Biphasic Ti-Ni-Sn Alloys for Use in Thermoelectric Applications. *J. Appl. Phys.* **2014**, *115*, 043720.

(43) Öğüt, S.; Rabe, K. M. Band Gap and Stability in the Ternary Intermetallic Compounds NiSnM M=Ti,Zr,Hf: A First-Principles Study. *Phys. Rev. B* **1995**, *51*, 10443–10453.

(44) Arushanov, E.; Kaefer, W.; Fess, K.; Kloc, C.; Friemelt, K.; Bucher, E. Transport Properties of n-ZrNiSn Single Crystals. *Phys. Status Solidi A* **2000**, *177*, 511–520.

(45) Ouardi, S.; Fecher, G. H.; Balke, B.; Kozina, X.; Stryganyuk, G.; Felser, C.; Lowitzer, S.; Ködderitzsch, D.; Ebert, H.; Ikenaga, E. Electronic Transport Properties of Electron- and Hole-Doped Semiconducting $C1_b$ Heusler Compounds: $NiTi_{1-x}M_xSn$ (M=Sc,V). *Phys. Rev. B* **2010**, *82*, 085108.

(46) Goldsmid, H. J.; Sharp, J. W. Estimation of the Thermal Band Gap of a Semiconductor from Seebeck Measurements. *J. Electron. Mater.* **1999**, *28*, 869–872.

(47) Cook, B.; Harringa, J.; Tan, Z.; Jesser, W. TiNiSn: A Gateway to the (1,1,1) Intermetallic Compounds. Fifteenth International Conference on Thermoelectrics, 1996. 1996; pp 122–127.

(48) Xie, H.; Wang, H.; Fu, C.; Liu, Y.; Snyder, G. J.; Zhao, X.; Zhu, T. The Intrinsic Disorder Related Alloy Scattering in ZrNiSn Half-Heusler Thermoelectric Materials. *Sci. Rep.* **2014**, *4*, 6888.

(49) Ziman, J. *Electrons and Phonons: The Theory of Transport Phenomena in Solids*; The International Series of Monographs on Physics; Clarendon Press, 1996; pp 288–292.

(50) Singh, D. J.; Terasaki, I. Thermoelectrics: Nanostructuring and More. *Nat. Mater.* **2008**, *7*, 616–617.